A Novel Pump-Pump-Probe Resonance Raman Approach Featuring Light-Induced Charge Accumulation on a Model Photosystem

Daniel H. Cruz Neto[a], Juan Soto[b], Nishith Maity[a], Christophe Lefumeux[a], Thai Nguyen[a], Pascal Pernot[c], Karine Steenkeste[a], Daniel Peláez[a], Minh-Huong Ha-Thi*[a], Thomas Pino*[a]*

[a]Institut des Sciences Moléculaires d'Orsay (ISMO), Université Paris-Saclay – CNRS ; 91405 Orsay, France

[b]Department of Physical Chemistry, Faculty of Science, University of Málaga; E-29071 Málaga, Spain

[c]Institut de Chimie Physique (ICP), Université Paris-Saclay, CNRS ; 91405 Orsay, France

Corresponding Authors

Daniel Peláez – daniel.pelaez-ruiz@universite-paris-saclay.fr

Minh-Huong Ha-Thi – minh-huong.ha-thi@universite-paris-saclay.fr

Thomas Pino – thomas.pino@universite-paris-saclay.fr

Abstract: Light-induced charge accumulation is at the heart of biomimetic systems aiming at solar fuel production in the realm of artificial photosynthesis. Understanding the mechanisms upon which these processes operate is a necessary condition to drive down the rational catalyst design road. We have built a nanosecond pump-pump-probe resonance Raman setup to witness the sequential charge accumulation process while probing vibrational features of different charge-separated states. By employing a reversible model system featuring methyl viologen (MV) as dual electron acceptor, we have been able to watch the photosensitized production of its neutral form, MV^0, resulting from two sequential electron transfer reactions. We have found that, upon double excitation, a fingerprint vibrational mode corresponding to the doubly reduced species appears at 992 cm^{-1} and peaks at 30 μs after the second excitation. This has been further confirmed by simulated resonance Raman spectra which fully support our experimental findings in this unprecedented build-up of charge seen by a resonance Raman probe.

TOC GRAPHICS

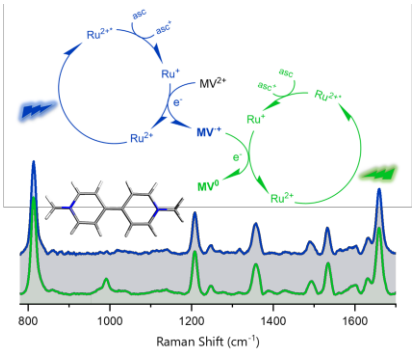

KEYWORDS: Artificial Photosynthesis. Charge Accumulation. Electron Transfer. Time-Resolved Raman Spectroscopy. Theoretical Resonance Raman Spectroscopy.

Nature's masterpiece of evolution, the photosynthetic process, provides energy to organisms through an arsenal of highly efficient light-powered transformations. Driven by humanity's colossal needs of sustainable energetic development, scientists have been attempting to take the leap towards artificial photosynthesis by employing the lessons learnt from its natural counterpart[1–4]. The blueprints of the natural process point out to a basic yet arduous requirement to march forward on this avenue: the light-driven accumulation of multiple redox equivalents and their exploitation on multi-electronic catalytic processes[1,3,5–8].

Indeed, natural organisms have evolved to master the ability of performing such thermodynamically challenging tasks[9,10], providing science with clues on how to engineer artificial systems capable of mimicking their subtleties. However, the development of such biomimetic prototypes requires a great deal of rational molecular design coupled with a thorough and accurate spectroscopic depiction of the fundamental photoinduced charge accumulation and catalytic processes they host.

Spectroscopic characterization of such photo-driven processes is oftentimes reliant upon the use of sacrificial reagents to skirt parasitic reactions[5,11–13]. Recent advances in reversible systems have allowed us to paint a more realistic picture of their full complexity, some of which were systematically reviewed by Bürgin and Wenger[6]. Experimentally, transient absorption spectroscopy is the primary technique capable of providing a real-time look into spectral and kinetic properties of such dynamic charge-accumulating systems[14,15], and it has allowed us to draw mechanistic insights from their behavior on different timescales.

Recently, some of us have demonstrated the possibility of probing accumulative charge separation by employing sequential pump-pump excitations on a biomimetic system containing methyl viologen[8], a common electron relay in photochemical studies[16–18]. This concept was also

applied to a similar system with naphthalene diimide and $[Ru(bpy)_3]^{2+}$ (bpy = 2,2'-bypiridine) in a dyad arrangement[19] and in a multicomponent configuration with sodium ascorbate as a reversible electron donor[20]. A bimetallic ruthenium-rhenium dyad with a modest catalytic activity for the reduction of CO_2 was also successfully investigated under double excitation[21], thus further consolidating this technique.

These successful applications of such sequential dual excitation strategy to probe the absorption of different charge-separated states have prompted us to look further into other complementary probing possibilities to detect transient species. This would be particularly beneficial for systems whose transient optical signatures are strongly overlapping, rendering their assignment rather difficult.

To that end, time-resolved resonance Raman spectroscopy (TR3) is an outstanding candidate, providing both structural and dynamical information on transient species[22] through their Raman-active vibrational modes. In addition, this technique comes with the striking possibility of probing photogenerated reactive intermediates, enabling us to take real-time snapshots of reaction mechanisms and catalytic cycles[23]. This is a prime prospect for the pursuits of artificial photosynthesis where information on structure-activity relationships are indispensable to the engineering of molecular catalysts.

Several examples of successful implementations of this technique to study electron transfer reactions have already been published[24–27], and, most recently, our group has reported the reversible, photosensitized one-electron reduction of the methyl viologen dication (MV^{2+}) to its radical cation form ($MV^{\cdot+}$) under laboratory pump-probe conditions tracked by resonance-enhanced, Raman-active vibrational modes[28].

In this communication, we take a step forward on these studies by demonstrating the application of a novel nanosecond pump-pump-probe resonance Raman experimental approach featuring the reversible, photosensitized, and sequential 2-electron accumulation on MV^{2+} to yield its neutral form (MV^0). Herein, the system under scrutiny is analogous to our previous report[8] – MV^{2+} (13.4 μM) as the electron acceptor, $[Ru(bpy)_3]^{2+}$ (86 μM) as the photosensitizer, and ascorbate (100 mM) as the reversible electron donor in deaerated CH_3CN:H_2O (6:4). The resonance Raman oxidation-state-specific vibrational modes of the radical cation and the neutral species have been calculated in accordance with the vibronic theory of Albrecht[29–31], modified by a multi-state version[32,33] which considers only Franck-Condon factors. (TD-)DFT calculations using the CAM-B3LYP[34]/def2-TZVPP[35] level of theory have been employed for this. The small displacement approximation and the independent mode displaced harmonic oscillator (IMDHO) models have been assumed in our calculations. The vibrational analysis in internal coordinates has been performed following the *GF* formalism of Wilson[36–38]. A comprehensive description of the experimental techniques and the theoretical approaches is presented in the Supporting Information.

The nanosecond pump-pump-probe resonance Raman experimental setup is detailed in Figure S1. In short, two laser pumps (480 and 532 nm) are sent to excite the sample and a third laser (395 nm) is used to probe the Raman scattering signals. The delay times amongst the individual pumps and the probe are electronically controlled, thus rendering the measurements time-resolved. The probe wavelength was chosen to match the overlapping electronic transitions observed for both $MV^{\cdot+}$ and MV^0 (see absorption spectra in Figure S7)[39], ergo allowing operation under resonant conditions, while the pumps had their energies adjusted to excite the $[Ru(bpy)_3]^{2+}$ complex with approximately the same efficiency.

Excitation of the photosensitizing complex leads to the classical activation of the system – light absorption by $[Ru(bpy)_3]^{2+}$ followed by reductive quenching of its ^{3}MLCT excited state in the presence of excess ascorbate, forming $[Ru(bpy)_3]^{+}$ (denoted Ru^{+})[8,20]. Since these are the very first transient events leading to charge accumulation, single flash TR3 measurements were performed in the absence of MV^{2+} to unravel possible contributions from transient species formed in these steps. Although a clear formation of Ru^{+} can be seen in transient absorption with a rising band centered at 510 nm (Figure S8), its formation in TR3, together with oxidized ascorbate (denoted asc^{+}), seems to be silent or at least indiscernible (Figure S18). This observation is not surprising, and it can be rationalized by the fact that the Raman signals coming from both photogenerated intermediates are not enhanced by resonance under our experimental conditions.

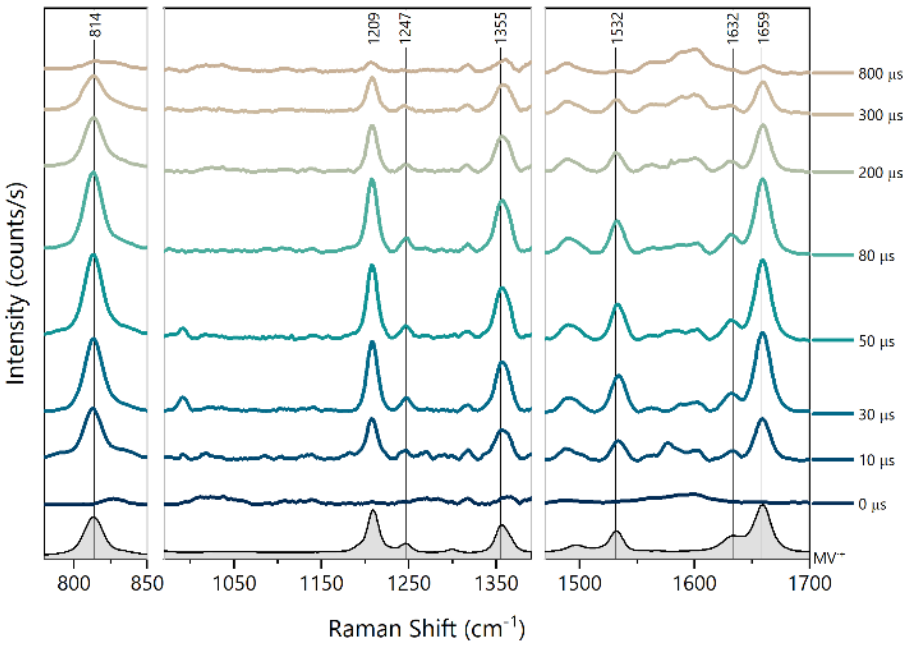

Figure 1. Single flash TR3 of the mixture MV^{2+} (13.4 µM), $[Ru(bpy)_3]^{2+}$ (86 µM), and ascorbate (100 mM) in deaerated CH_3CN:H_2O (6:4), showcasing the formation and decay of $MV^{\cdot+}$. The spectra were recorded at the indicated delay times and the vibrational bands are assigned according

to a laboratory reference of $MV^{\cdot+}$ (solid lines); λ_{pump} = 532 nm – 4.5 mJ/pulse, λ_{probe} = 395 nm – 1.1 mJ/pulse.

The same single flash TR3 measurements performed in the presence of MV^{2+}, however, result in the formation of intense, well-resolved bands of $MV^{\cdot+}$, product of the first light-induced electron transfer from Ru^{+} to MV^{2+} (Figure 1). The main strong signals corresponding to the radical cation appear at 814, 1209, 1355, 1532, and 1659 cm^{-1} in the spectral window selected. A scaled reference spectrum of $MV^{\cdot+}$ obtained by Raman spectro-electrochemical measurements (SEC, Figure S14) is also included in Figure 1 for comparison, unquestionably confirming that the newly-formed bands result from the first electron transfer reaction. The characteristic vibrational modes of $MV^{\cdot+}$ have previously been reported[28,40–42] and their assignment is available in Table 1 together with their DFT harmonic frequencies. The theoretical methodology employed herein allowed for an unambiguous assignment of the vibrations as the calculated spectra reproduce well the bands observed in the experiments.

Complementarily, the transient absorption of the system was probed under single pump excitation (Figure S10), and the time evolution of the pure signal corresponding to $MV^{\cdot+}$ in transient absorption and TR3 (605 nm and 1355 cm^{-1}, respectively) are shown to follow the same kinetics (Figure S19), with the radical cation concentration peaking at ~80 μs. The kinetic trace was successfully simulated with a formation rate constant of 3.5 (±1.0) $x10^{9}$ $M^{-1}s^{-1}$. One important feature to be noted in the TR3 spectra presented in Figure 1, particularly at 30 and 50 μs, is the presence of a new band at 992 cm^{-1}. This signal is assigned to MV^{0} (see reference spectra, Figure S14) and, surprisingly, it indicates that charge accumulation is already observed with a single pump excitation due to two sequential single-photon absorption processes, a phenomenon that seems to be recurrent in such multicomponent systems[20]. The possibility of MV^{0} being formed due

to disproportionation of $MV^{\cdot+}$ was ruled out by kinetics simulations of the experimental decays, which have shown to not be compatible with a disproportionation mechanistic step. Naturally, the amount of MV^0 formed due to the single pump is low, so that a robust accumulation strategy is needed.

Our game plan consists in re-exciting the sample with a second pump delayed by 80 µs, strategically regenerating Ru^+ when the solution has the highest possible concentration of $MV^{\cdot+}$, thus favoring the reduction of the latter to yield its neutral form. The time-resolved spectra presented in Figure 2, obtained after the second pump excitation, clearly showcase the rising and decay of a new vibrational mode centered at 992 cm^{-1}. A comparison with the reference spectrum obtained for MV^0 is presented and, remarkably, we can already attribute the new band to the formation of the neutral species.

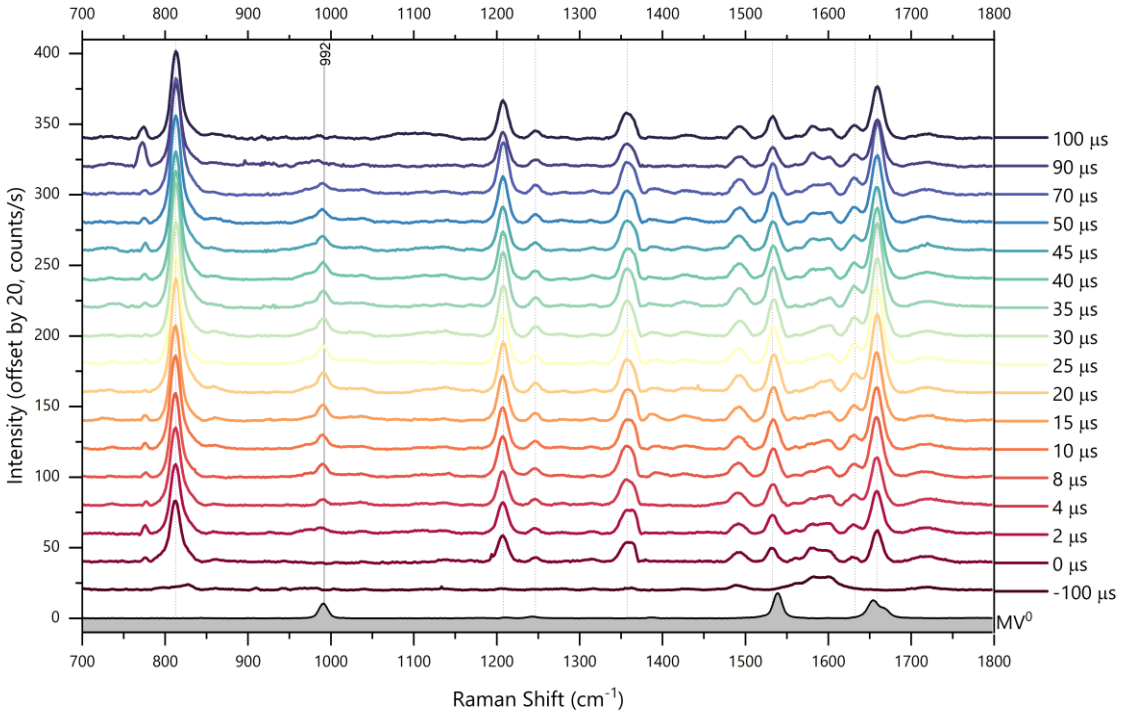

Figure 2. Double flash TR3 spectra of a solution containing MV^{2+} (13.4 µM), $[Ru(bpy)_3]^{2+}$ (86 µM), and ascorbate (100 mM) in deaerated CH_3CN:H_2O (6:4) at selected delay times after the

second pump. The time-evolving band at 992 cm^{-1} (solid line) indicates the light-induced formation of neutral methyl viologen (MV^0). A reference spectrum of MV^0, obtained from Raman SEC, is included in the dataset for comparison. The bands of $MV^{\cdot+}$ are also highlighted (dotted lines). The spectra were recorded with λ_{pump1} = 480 nm – 0.8 mJ/pulse, λ_{pump2} = 532 nm – 4.6 mJ/pulse, λ_{probe} = 395 nm – 1.0 mJ/pulse, with a delay of 80 μs between the pumps, and corrected for sequential single-photon absorption processes leading to the formation of MV^0 (details in SI).

The other intense vibrational signatures of MV^0 observed at 1538 and 1654 cm^{-1} have a significant overlap with the corresponding signals of $MV^{\cdot+}$ (Figure S14), so that they appear as a small contribution to the dominating bands of the radical cation, also formed with the second pump. Indeed, due to the contribution of MV^0, the intensity ratio I_{1538}/I_{814} (814 cm^{-1} is the pure $MV^{\cdot+}$ band) increases by nearly 50% from 0 to 30 μs, the latter being the delay time at which the highest intensity of MV^0 is observed. Figure 2 also contains the spectrum obtained at a negative delay time, i.e., -100 μs, showing only contributions of $[Ru(bpy)_3]^{2+}$, ascorbate, and MV^{2+}, none of which were in resonance with the Raman probe.

A summary of the most intense vibrational frequencies detected in the time-resolved experiments is displayed in Table 1, together with the calculated DFT harmonic frequencies and the corresponding assignment of each vibrational mode. In the literature, the fingerprint band of MV^0, recorded at 992 cm^{-1}, had been previously assigned to ring breathing[41] and to out-of-plane bending of the ring carbon atoms[42]. In contrast, our DFT calculations (see Table S4), in agreement with a previous study[43], indicate that this totally symmetric vibrational mode should be more appropriately assigned to a ring torsion (see Tables S2 and S4).

Table 1. Vibrational frequencies (in cm^{-1}) of the main peaks observed in Single Flash (SF) and Double Flash (DF) TR3 experiments assigned to $MV^{\cdot+}$ and MV^0, respectively. Literature values, as well as those obtained from DFT at the CAM-B3LYP/def2-TVZPP (not scaled) level are added for comparison.

$MV^{\cdot+}$			MV^0			
SF-TR3	Lit.[a]	Theo.[b]	DF-TR3	Lit.[a]	Theo.[b]	Assignment[c]
814	817[41,42] 814[28]	844			814	Ring breathing (1)
			992	996[41,42]	1027	Ring torsion
1209	1212[41,42] 1214[28]	1255	1211	1214[41]	1255	C-H rocking (9a)
1355	1357[41], 1351[28,42]	1407				C-H rocking (3) + C-C inter-ring stretching
1532	1532[41,42] 1545[28]	1592	1538	1538[42] 1543[41]	1639	C-C inter-ring stretching
1659	1662[41] 1658[28,42]	1744	1654	1656[42] 1659[41]	1763	C-C ring stretching (8a)

[a] Literature values for comparison. [b] This work (unscaled). [c] Assignment of vibrational modes with Wilson's notation in parenthesis[44]

Although in TR3 the formation of MV^0 can be readily seen due to the unique normal mode at 992 cm^{-1}, the same cannot be said about the measurements with an absorption probe. That is because the transient absorption signal observed at 395 nm in double flash experiments contains both the contributions of $MV^{\cdot+}$ and MV^0 (Figure S7). Luckily, for the methyl viologen system, the absorption feature of $MV^{\cdot+}$ at 605 nm in the single flash experiment can be used to correct the double flash signal and to obtain the spectrum of MV^0 for each delay time. This was done in both our previous work[8] and in this paper (Figure S13). Still, the possibility of observing the second charge-separated state in TR3 without relying on data treatment methodologies demonstrates the

startling capabilities of vibrational spectroscopy in the study of photogenerated charge-separated states, as well as the complementarity between both double flash experiments for a detailed structural and dynamical description of sequential charge accumulation in reversible biomimetic systems.

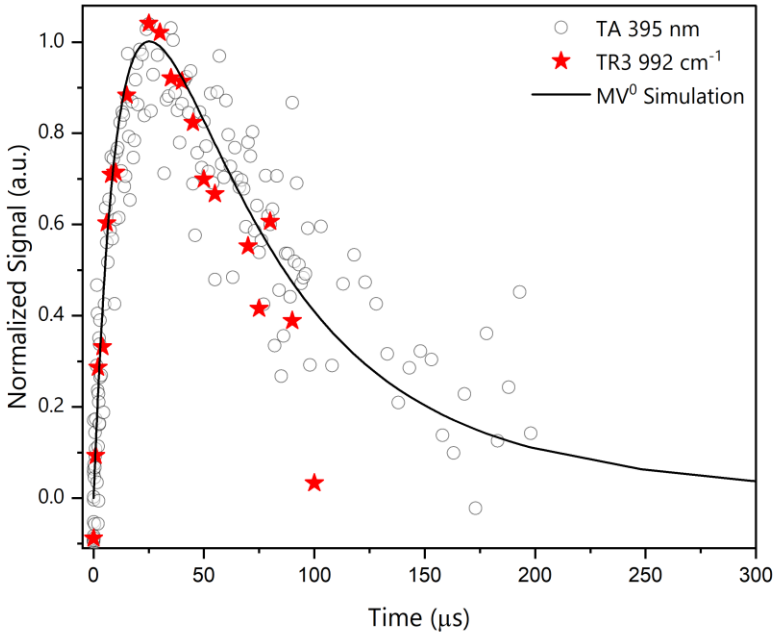

Figure 3. Corrected and normalized kinetic traces of MV^0 obtained with double flash excitations in transient absorption (395 nm) and TR3 (992 cm^{-1}) spectroscopies. Simulation of the kinetics represented in the solid line.

The time-resolved measurements also allow us to distil information on the pure kinetics of formation and decay of MV^0. Figure 3 shows the normalized overlap between the kinetic curves of MV^0 observed in transient absorption (395 nm), and TR3 (992 cm^{-1}), together with the simulation of the second order reactions, which was performed on the SK-ANA software[45]. The formation of MV^0 was simulated with k_{ET2} of 2.5 (±0.8) x10^9 $M^{-1}s^{-1}$ and the decay with k_{rec} of 1.5

(±0.5) x10^9 $M^{-1}s^{-1}$, in accordance with previously published results[8]. The rising of the signal is due to the electron transfer reaction between $MV^{\cdot+}$ and Ru^+, yielding MV^0, while the decay comes from the recombination of the latter with asc^+. Once again, we show that the decays measured by double flash under transient optical absorption and Raman probes reasonably follow the same kinetics. This further confirms that the same processes are being looked at through the lenses of different and complementary approaches.

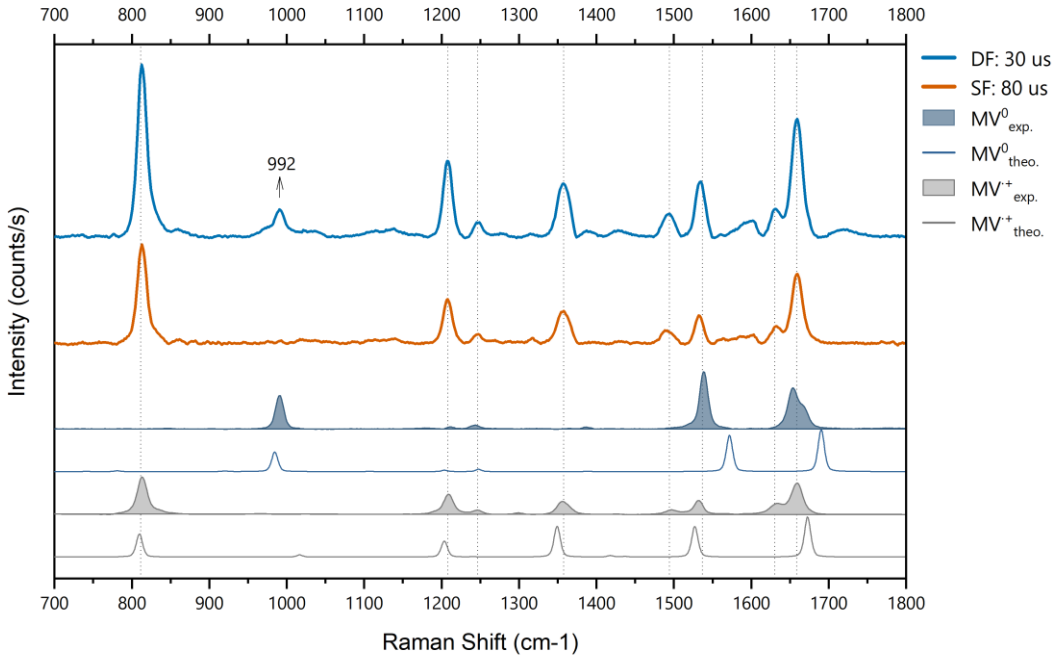

Figure 4. TR3 spectra recorded at the delay times in which the first and second charge-separated states are observed upon single (SF 80 µs) and double (DF 30 µs) flash excitations, respectively. The mixture was composed of MV^{2+} (13.4 µM), $[Ru(bpy)_3]^{2+}$ (86 µM), and ascorbate (100 mM) in deaerated CH_3CN:H_2O (6:4). Laboratory references of $MV^{\cdot+}$ (plain blue curve) and MV^0 (plain grey curve) are included for comparison, as well as our simulated resonant Raman spectra.

In addition, we find that MV^0 has its highest concentration in solution approximately 30 μs after the second excitation. A summary of all photoinduced transient events investigated herein is presented in the energy diagram depicted in Figure S20. The rate constants have been reported elsewhere[8], and here we focus on the detection and characterization of charge-separated states.

An overview of all spectral features recorded in our experiments is shown in Figure 4. Reference resonance Raman SEC measurements undoubtedly confirmed the formation of $MV^{\cdot+}$ and MV^0, with fingerprint vibrational modes observed at 1355 cm^{-1} and 992 cm^{-1}, respectively. Our simulated resonant Raman spectra successfully reproduced the frequencies and relative intensities of the vibrational bands for both reduced states of methyl viologen, allowing us to look deeper into their character. The totally symmetric character of all vibrational modes obtained for both species (as in the simulation), is also confirmed with steady-state measurements of resonant Raman intensities under parallel and perpendicular polarizations (Figures S16 and S17).

In conclusion, we have developed a novel nanosecond pump-pump-probe resonance Raman experimental setup devoted to investigating photoinduced sequential charge accumulation processes. The possibility of tracking the reversible, photosensitized charge build-up on methyl viologen with a resonance Raman probe is demonstrated for the first time. Such vibrational spectroscopy technique is particularly suited to inspect structural rearrangements resulting from electron transfers and can provide new insights in the mechanistic routes of photocatalytic reactions. In the ever-growing field of artificial photosynthesis and solar energy production, experimental tools to interrogate mechanisms of charge separation and accumulation are fundamental for the rational design and optimization of artificial biomimetic systems.

ASSOCIATED CONTENT

Supporting Information

Detailed experimental and theoretical methodologies employed for data acquisition and treatment, pump-pump-probe resonance Raman setup, supplementary steady-state and time-resolved reference measurements, theoretical spectra and analysis of theoretical harmonic frequencies.

AUTHOR INFORMATION

Corresponding authors

Daniel Peláez – Institut des Sciences Moléculaires d'Orsay (ISMO), Université Paris-Saclay – CNRS ; 91405 Orsay, France. E-mail: daniel.pelaez-ruiz@universite-paris-saclay.fr

Minh-Huong Ha-Thi – Institut des Sciences Moléculaires d'Orsay (ISMO), Université Paris-Saclay – CNRS ; 91405 Orsay, France. E-mail: minh-huong.ha-thi@universite-paris-saclay.fr

Thomas Pino – Institut des Sciences Moléculaires d'Orsay (ISMO), Université Paris-Saclay – CNRS ; 91405 Orsay, France. E-mail: thomas.pino@universite-paris-saclay.fr

Notes

The authors declare no competing financial interests.

ACKNOWLEDGMENT

This research has been supported by the French National Research Agency (LOCO, grant N. ANR-19-CE05-0020-02). DFT calculations performed using computational resources from the Moulon Mésocentre – Ruche. DHCN and DP gratefully acknowledge the computational support

by Andrei Borissov (ISMO) and Jean-Yves Bazarra (ISMO). DHCN is grateful for the MESRI grant (2021-2024). We thank Paris-Saclay University and CNRS for additional financial support.

REFERENCES

(1) Balzani, V.; Credi, A.; Venturi, M. Photochemical Conversion of Solar Energy. *ChemSusChem*. **2008**, *1*, 26-58.

(2) Gotico, P.; Roupnel, L.; Guillot, R.; Sircoglou, M.; Leibl, W.; Halime, Z.; Aukauloo, A. Atropisomeric Hydrogen Bonding Control for CO2 Binding and Enhancement of Electrocatalytic Reduction at Iron Porphyrins. *Angew. Chemie - Int. Ed.* **2020**, *59* (50), 22451–22455.

(3) Gust, D.; Moore, T. A.; Moore, A. L. Solar Fuels via Artificial Photosynthesis. *Acc. Chem. Res.* **2009**, *42* (12), 1890–1898.

(4) Puntoriero, F.; Ishitani, O. Metal Complexes and Inorganic Materials for Solar Fuel Production. *Dalt. Trans.* **2020**, *49* (20), 6529–6531.

(5) Hammarström, L. Accumulative Charge Separation for Solar Fuels Production: Coupling Light-Induced Single Electron Transfer to Multielectron Catalysis. *Acc. Chem. Res.* **2015**, *48* (3), 840–850.

(6) Bürgin, T. H.; Wenger, O. S. Recent Advances and Perspectives in Photodriven Charge Accumulation in Molecular Compounds: A Mini Review. *Energy and Fuels* **2021**, *35* (23), 18848–18856.

(7) Nomrowski, J.; Guo, X.; Wenger, O. S. Charge Accumulation and Multi-Electron Photoredox Chemistry with a Sensitizer–Catalyst–Sensitizer Triad. *Chem. – A Eur. J.* **2018**, *24* (53), 14084–14087.

(8) Tran, T. T.; Ha-Thi, M. H.; Pino, T.; Quaranta, A.; Lefumeux, C.; Leibl, W.; Aukauloo, A.

Snapshots of Light Induced Accumulation of Two Charges on Methylviologen Using a Sequential Nanosecond Pump-Pump Photoexcitation. *J. Phys. Chem. Lett.* **2018**, *9* (5), 1086–1091.

(9) Pellegrin, Y.; Odobel, F. Molecular Devices Featuring Sequential Photoinduced Charge Separations for the Storage of Multiple Redox Equivalents. *Coord. Chem. Rev.* **2011**, *255* (21–22), 2578–2593.

(10) Dau, H.; Zaharieva, I. Principles, Efficiency, and Blueprint Character of Solar-Energy Conversion in Photosynthetic Water Oxidation. *Acc. Chem. Res.* **2009**, *42* (12), 1861–1870.

(11) Lefebvre, J. F.; Schindler, J.; Traber, P.; Zhang, Y.; Kupfer, S.; Gräfe, S.; Baussanne, I.; Demeunynck, M.; Mouesca, J. M.; Gambarelli, S.; Artero, V.; Dietzek, B.; Chavarot-Kerlidou, M. An Artificial Photosynthetic System for Photoaccumulation of Two Electrons on a Fused Dipyridophenazine (Dppz)–Pyridoquinolinone Ligand. *Chem. Sci.* **2018**, *9* (17), 4152–4159.

(12) Berardi, S.; Drouet, S.; Francàs, L.; Gimbert-Suriñach, C.; Guttentag, M.; Richmond, C.; Stoll, T.; Llobet, A. Molecular Artificial Photosynthesis. *Chem. Soc. Rev.* **2014**, *43* (22), 7501–7519.

(13) Bonn, A. G.; Wenger, O. S. Photoinduced Charge Accumulation in Molecular Systems. *Chimia (Aarau).* **2015**, *69* (1–2), 17-21.

(14) Berera, R.; van Grondelle, R.; Kennis, J. T. M. Ultrafast Transient Absorption Spectroscopy: Principles and Application to Photosynthetic Systems. *Photosynth. Res.* **2009**, *101* (2–3), 105–118.

(15) Miao, T. J.; Tang, J. Characterization of Charge Carrier Behavior in Photocatalysis Using Transient Absorption Spectroscopy. *J. Chem. Phys.* **2020**, *152* (19), 1-11.

(16) Lomoth, R.; Häupl, T.; Johansson, O.; Hammarström, L. Redox-Switchable Direction of Photoinduced Electron Transfer in an $Ru(Bpy)_3^{2+}$-Viologen Dyad. *Chem. - A Eur. J.* **2002**, *8* (1), 102–110.

(17) Suzuki, M.; Morris, N. D.; Mallouk, T. E. Photosensitized Production of Doubly Reduced Methylviologen Followed by Highly Efficient Methylviologen Radical Formation Using Self-Assembling Ruthenium(II) Complexes. *Chem. Commun.* **2002**, *2* (14), 1534–1535.

(18) Ogawa, T.; Nishikawa, H. Poly(Vinyl Alcohol) Film Containing Methyl Viologen as a Highly Sensitive Dosimeter. *Int. J. of Radiat. Appl. Instrum. Part C.* **1987**, *29* (5), 353–357.

(19) Mendes Marinho, S.; Ha-Thi, M. H.; Pham, V. T.; Quaranta, A.; Pino, T.; Lefumeux, C.; Chamaillé, T.; Leibl, W.; Aukauloo, A. Time-Resolved Interception of Multiple-Charge Accumulation in a Sensitizer–Acceptor Dyad. *Angew. Chemie - Int. Ed.* **2017**, *56* (50), 15936–15940.

(20) Tran, T. T.; Pino, T.; Ha-Thi, M. H. Watching Intermolecular Light-Induced Charge Accumulation on Naphthalene Diimide by Tris(Bipyridyl)Ruthenium(II) Photosensitizer. *J. Phys. Chem. C* **2019**, *123* (47), 28651–28658.

(21) Gotico, P.; Tran, T. T.; Baron, A.; Vauzeilles, B.; Lefumeux, C.; Ha-Thi, M. H.; Pino, T.; Halime, Z.; Quaranta, A.; Leibl, W.; Aukauloo, A. Tracking Charge Accumulation in a Functional Triazole-Linked Ruthenium-Rhenium Dyad Towards Photocatalytic Carbon Dioxide Reduction. *ChemPhotoChem.* **2021**, *5* (7), 654–664.

(22) Bell, S. E. J. Tutorial Review. Time-Resolved Resonance Raman Spectroscopy. *Analyst* **1996**, *121*, 107R-120R.

(23) Sahoo, S. K.; Umapathy, S.; Parker, A. W. Time-Resolved Resonance Raman Spectroscopy: Exploring Reactive Intermediates. *Appl. Spectrosc.* **2011**, *65* (10), 1087–

1115.

(24) Mohapatra, H.; Umapathy, S. Influence of Solvent on Photoinduced Electron-Transfer Reaction: Time-Resolved Resonance Raman Study. *J. Phys. Chem. A* **2009**, *113* (25), 6904–6909.

(25) Mohapatra, H.; Umapathy, S. Time-Resolved Resonance Raman Spectroscopic Studies on the Radical Anions of Methyl-1,4-Benzoquinone and 2,6-Dimethyl-1,4-Benzoquinone. *J. Phys. Chem. A* **2002**, *106* (18), 4513–4518.

(26) Ma, J.; Su, T.; Li, M. De; Du, W.; Huang, J.; Guan, X.; Phillips, D. L. How and When Does an Unusual and Efficient Photoredox Reaction of 2-(1-Hydroxyethyl) 9,10-Anthraquinone Occur? A Combined Time-Resolved Spectroscopic and DFT Study. *J. Am. Chem. Soc.* **2012**, *134* (36), 14858–14868.

(27) Forster, M.; Hester, R. Resonance Raman Investigation of the Photoreduction of Methylviologen with $Ru(Bpy)_3^{2+}$ and Proflavine as Sensitizers. *Chem. Phys. Lett.* **1982**, *85* (3), 287–292.

(28) Hammonds, M.; Tran, T. T.; Tran, Y. H. H.; Ha-Thi, M. H.; Pino, T. Time-Resolved Resonant Raman Spectroscopy of the Photoinduced Electron Transfer from Ruthenium(II) Trisbipyridine to Methyl Viologen. *J. Phys. Chem. A* **2020**, *124* (14), 2736–2740.

(29) Albrecht, A. C. On the Theory of Raman Intensities. *J. Chem. Phys.* **1961**, *34* (5), 1476–1484.

(30) Clark, R. J. H.; Dines, T. J. Resonance Raman Spectroscopy and Its Application in Bioinorganic Chemistry. In *Practical Approaches to Biological Inorganic Chemistry (2nd Ed)*. Elsevier, 2020. pp. 275-324.

(31) Long, D. A. *The Raman Effect: A Unified Treatment of the Theory of Raman Scattering by*

Molecules; John Wiley & Sons, 2002.

(32) Lopez-Ramirez, M. R.; Aranda Ruiz, D.; Avila Ferrer, F. J.; Centeno, S. P.; Arenas, J. F.; Otero, J. C.; Soto, J. Analysis of the Potential Dependent Surface-Enhanced Raman Scattering of p-Aminothiophenol on the Basis of MS-CASPT2 Calculations. *J. Phys. Chem. C* **2016**, *120* (34), 19322–19328.

(33) Aranda, D.; Avila, F. J.; López-Tocón, I.; Arenas, J. F.; Otero, J. C.; Soto, J. An MS-CASPT2 Study of the Photodecomposition of 4-Methoxyphenyl Azide: Role of Internal Conversion and Intersystem Crossing. *Phys. Chem. Chem. Phys.* **2018**, *20* (11), 7764–7771.

(34) Yanai, T.; Tew, D. P.; Handy, N. C. A New Hybrid Exchange–Correlation Functional Using the Coulomb-Attenuating Method (CAM-B3LYP). *Chem. Phys. Lett.* **2004**, *393* (1–3), 51–57.

(35) Weigend, F.; Ahlrichs, R.; Gmbh, F. K. Balanced Basis Sets of Split Valence, Triple Zeta Valence and Quadruple Zeta Valence Quality for H to Rn: Design and Assessment of Accuracy. *Phys. Chem. Chem. Phys.* **2005**, *7*, 3297–3305.

(36) Wilson, E. B.; Decius, J. C.; Cross, P. C. *Molecular Vibrations: The Theory of Infrared and Raman Vibrational Spectra*; MacGraw-Hills, 1955.

(37) Arenas, J. F.; Centeno, S. P.; Marcos, J. I.; Otero, J. C.; Soto, J. A Method to Improve the Agreement between Calculated and Observed Vibrational Frequencies after Scaling of a Quantum Mechanical Force Field. *J. Chem. Phys.* **2000**, *113* (19), 8472–8477.

(38) Soto, J.; Algarra, M.; Peláez, D. Nitrene Formation Is the First Step of the Thermal and Photochemical Decomposition Reactions of Organic Azides. *Phys. Chem. Chem. Phys.* **2022**, *24* (8), 5109–5115.

(39) Watanabe, T.; Honda, K. Measurement of the Extinction Coefficient of the Methyl

Viologen Cation Radical and the Efficiency of Its Formation by Semiconductor Photocatalysis. *J. Phys. Chem.* **1982**, *86* (14), 2617–2619.

(40) Poizat, O.; Sourisseau, C.; Mathey, Y. Vibrational Study of the Methyl Viologen Dication MV^{2+} and Radical Cation $MV^{\cdot+}$ in Several Salts and as an Intercalate in Some Layered MPS3 Compounds. *J. Chem. Soc. Faraday Trans. 1 Phys. Chem. Condens. Phases* **1984**, *80* (12), 3257–3274.

(41) Feng, Q.; Cotton, T. M. A Surface-Enhanced Resonance Raman Study of the Photoreduction of Methylviologen on a p-InP Semiconductor Electrode. *J. Phys. Chem.* **1986**, *90* (6), 983–987.

(42) Lu, T.; Birke, R. L.; Lombardi, J. R. Surface Raman Spectroscopy of the Three Redox Forms of Methylviologen. *Langmuir* **1986**, *2* (3), 305–309.

(43) Romanova, J.; Liégeois, V.; Champagne, B. Resonant Raman Spectra of Molecules with Diradical Character: Multiconfigurational Wavefunction Investigation of Neutral Viologens. *Phys. Chem. Chem. Phys.* **2014**, *16* (39), 21721–21731.

(44) E. Bright Wilson; Jr. The Normal Modes and Frequencies of Vibration of the Regular Plane Haxagon Model of the Benzene Molecule. *Phys. Rev.* **1934**, *853* (1923), 669–670.

(45) Pernot, P. *ppernot/SK-Ana: Asynchronous processes (v3.4)*. 2022. Zenodo.